Supporting Information: High Spatial and Temporal Resolution Synthetic Aperture Phase Microscopy (HISTR-SAPM)

*Cheng Zheng[1,2], Di Jin[3], Yanping He[1], Hongtao Lin[4], Juejun Hu[5], Zahid Yaqoob[6], Peter T. C. So[2,6,7], Renjie Zhou[1,8]**

[1]Department of Biomedical Engineering, The Chinese University of Hong Kong, Shatin, New Territories, Hong Kong, China

[2]Department of Mechanical Engineering, Massachusetts Institute of Technology, Cambridge, Massachusetts 02139, USA

[3]Computer Science and Artificial Intelligence Laboratory, Massachusetts Institute of Technology, Cambridge, Massachusetts 02139, USA

[4]College of Information Science & Electronic Engineering, Zhejiang University, Hangzhou, China

[5]Department of Materials Science and Engineering, Massachusetts Institute of Technology, Cambridge, Massachusetts 02139, USA

[6]Laser Biomedical Research Center, Massachusetts Institute of Technology, Cambridge, MA 02139, USA

[7]Department of Biological Engineering, Massachusetts Institute of Technology, Cambridge, Massachusetts 02139, USA

[8]Shun Hing Institute of Advanced Engineering, The Chinese University of Hong Kong, Shatin, Hong Kong, China

Note S1: Lee holograms

The binary hologram patterns are described as:

$$h(x,y)=\frac{1}{2}\left\{1+\cos\left[2\pi\left(ux+vy\right)+\phi(x,y)\right]\right\}, \tag{S1}$$

where u and v are carrier frequencies along x and y axis, $\phi(x,y)$ is the encoded phase distribution, which is a 2D linear function whose slop determines the tilting angle of the generated plane wave. The carrier frequencies u and v values are chosen to provide enough separation between the 0th and 1st diffraction orders to avoid crosstalk. Then we apply a threshold (usually set as 0.5) to transfer $h(x,y)$ into a binary hologram for display on DMD1.

Note S2: Synthetic reconstruction

Under normal illumination, the sample beam $U_S(\mathbf{r})$ interferes with a tilted reference plane wave $U_R e^{i\mathbf{k_R}\cdot\mathbf{r}}$. At the imaging plane $\mathbf{r}_\perp=(x,y)$, the recorded interferogram is the intensity of the coherent addition of the two beams:

$$I(\mathbf{r}_\perp)=\left|U_S(\mathbf{r}_\perp)+U_R e^{i\mathbf{k}_{\mathbf{R}\perp}\cdot\mathbf{r}_\perp}\right|^2 , \tag{S2}$$

where $\mathbf{k}_{\mathbf{R}\perp}$ is the projection of reference wavevector on the imaging plane. By performing spatial Fourier transform, we can link the sample beam spatial spectrum $\tilde{U}_S(\mathbf{k}_\perp)$ with the measured interferogram as:

$$\tilde{I}(\mathbf{k}_\perp)=\tilde{U}_{DC}(\mathbf{k}_\perp)+U_R\tilde{U}_S(\mathbf{k}_\perp-\mathbf{k}_{\mathbf{R}\perp})+U_R\tilde{U}_S^*(-\mathbf{k}_\perp-\mathbf{k}_{\mathbf{R}\perp}) , \tag{S3}$$

where $\tilde{U}_{DC}(\mathbf{k}_\perp)=\mathbb{F}\left\{\left|U_S(\mathbf{r}_\perp)\right|^2+\left|U_R\right|^2\right\}$, $\tilde{U}_S(\mathbf{k}_\perp)=\mathbb{F}\{U_S(\mathbf{r}_\perp)\}$, and $\mathbb{F}$ denotes the 2D Fourier transform operation. Due to the tilted reference beam, fringes would form in the recorded interferogram

(Figure 1(a)-(i)), which will shift the sample beam spatial spectrum by $\mathbf{k}_{\mathbf{R}\perp}$ away from the origin, as shown in Figure 1(b)-(iv). Therefore, a bandpass filter, centered at $\mathbf{k}_{\mathbf{R}\perp}$ with a radius of NA_{det}/λ (NA_{det} is the detection objective numerical aperture), indicated by the dotted circle, can be used to extract the complex sample spatial spectrum corresponding to the term $U_R\tilde{U}_S\left(\mathbf{k}_\perp - \mathbf{k}_{\mathbf{R}\perp}\right)$ in Eq S3. After shifting the extracted complex sample spatial spectrum to the origin, we obtain the detected sample spatial spectrum $\tilde{U}_S\left(\mathbf{k}_\perp\right)$ as shown in the white dotted circle in Figure 2(a). For oblique illumination beam with a wavevector of $\mathbf{k}_{\mathbf{S}\perp}$, the detected spatial spectrum is $\tilde{U}_S\left(\mathbf{k}_\perp - \mathbf{k}_{\mathbf{S}\perp}\right)$. Thus, the shift amount is determined by $\mathbf{k}_{\mathbf{R}\perp} + \mathbf{k}_{\mathbf{S}\perp}$. In Figure 2(a), the dotted gold and orange circle regions show the detected sample spatial spectrum due to two different oblique illumination angles. Considering the mismatches in the optical path length, a global constant frame-to-frame phase offset is calculated during the synthesis process . For the overlapping regions, its value is calculated as the average of all the spectra that co-occupy this region. We also take into account the spatial variant phase errors induced by the possible motion of the sample. After aperture synthesis, an expanded sample spatial spectrum with a radius of $NA_{det}/\lambda + NA_{scan}/\lambda$ is achieved. NA_{scan}, determined by the maximum scan angle of the illumination beam, is a fraction of the NA of objective lens OL1. Considering the mismatches in the optical path length, a global constant frame-to-frame phase offset is calculated during the synthesis process. For the overlapping regions, its value is calculated as the average of all the spectra that co-occupy this region. We also take into account the spatial variant phase errors induced by the possible motion of the sample. Finally, an inverse Fourier transform is performed to produce the complex sample field, from which a high-resolution amplitude map (Figure 2(b)) and a phase map (Figure 2(c)) are obtained.

Note S3: Sample preparation

The subwavelength photonics structure is fabricated in the following procedure: firstly, a $Ge_{23}Sb_7S_{70}$ glass film of 250 nm thickness was deposited on top of a glass cover by a thermal evaporation method. The subwavelength structure was defined by electron beam lithography (Elionix ELS-F125) using Microchem SU-8 2000.2 resist both as the negative electron beam resist and etch mask. Then the pattern was transferred into the $Ge_{23}Sb_7S_{70}$ chalcogenide glass film by reactive-ion dry etching (PlasmaTherm Inc.). The refractive index of the glass film is measured to be 2.30 at 561 nm wavelength.

Human RBCs were collected and diluted in Alsever's solution (Sigma Aldrich Inc., A3551, RI = 1.337). The RBC sample were not centrifuged and washed so it contained whole blood. A drop of RBC sample was sandwiched between two No 1 glass coverslips before measurement.

COS-7, HeLa and NIH/3T3 cells were cultured in high-glucose Dulbecco's Modified Eagles Medium (DMEM) (GIBCO) supplemented with 10% fetal bovine serum (FBS) (GIBCO) and 1% penicillin-streptomycin (PS) (GIBCO) in an incubator at 37 ℃ with 5% CO2 atmosphere to form the confluent monolayer.

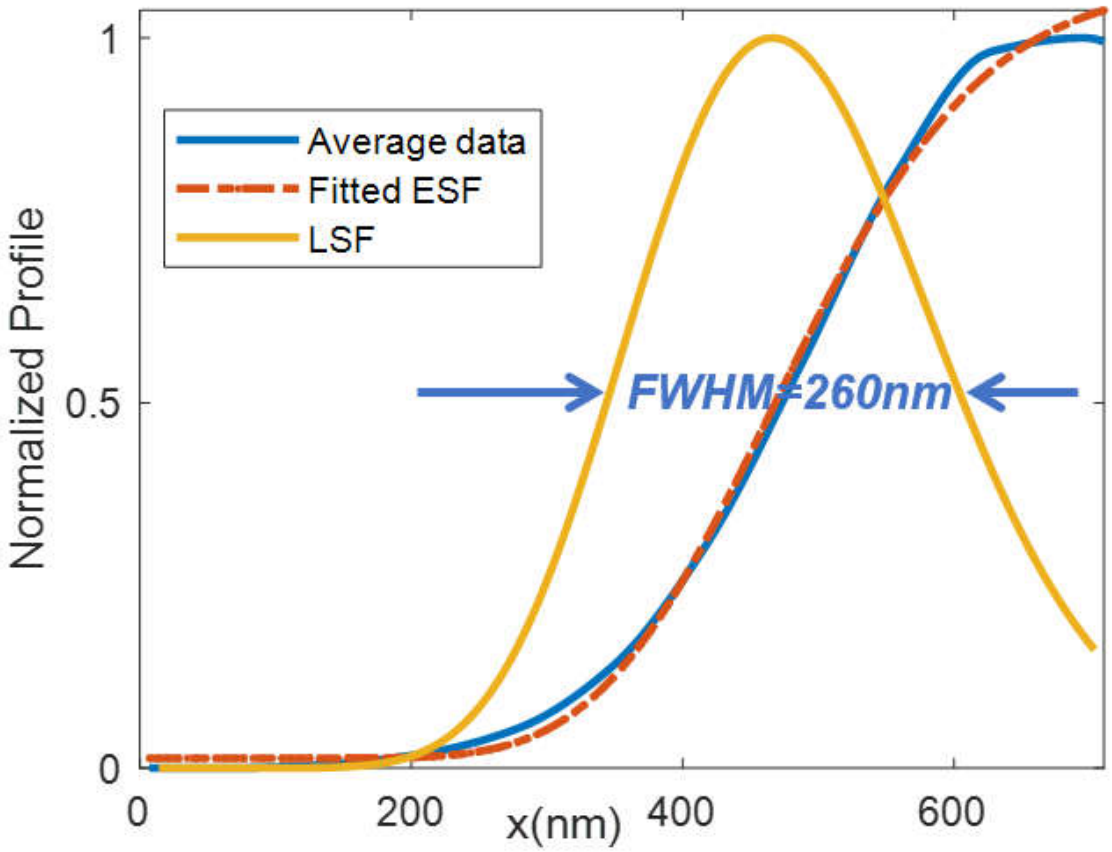

Figure S1. Lateral resolution verification with edge response. The average profile (blue line) along the edge of the largest line in Group 7 and Element 1 in the USAF resolution target (indicated by the white arrow in Fig. S2. (d)) is first plotted, and then fitted with an error function to obtain the edge spread function (ESF) (red dotted line). The lateral resolution is calculated as the FWHM of the line spread function (LSF), which is the derivative of the ESF. The FWHM is determined to be 260nm, which is in a good agreement the theoretical value of 233nm. Note that as the resolution criteria are different that will naturally result in slightly different values.

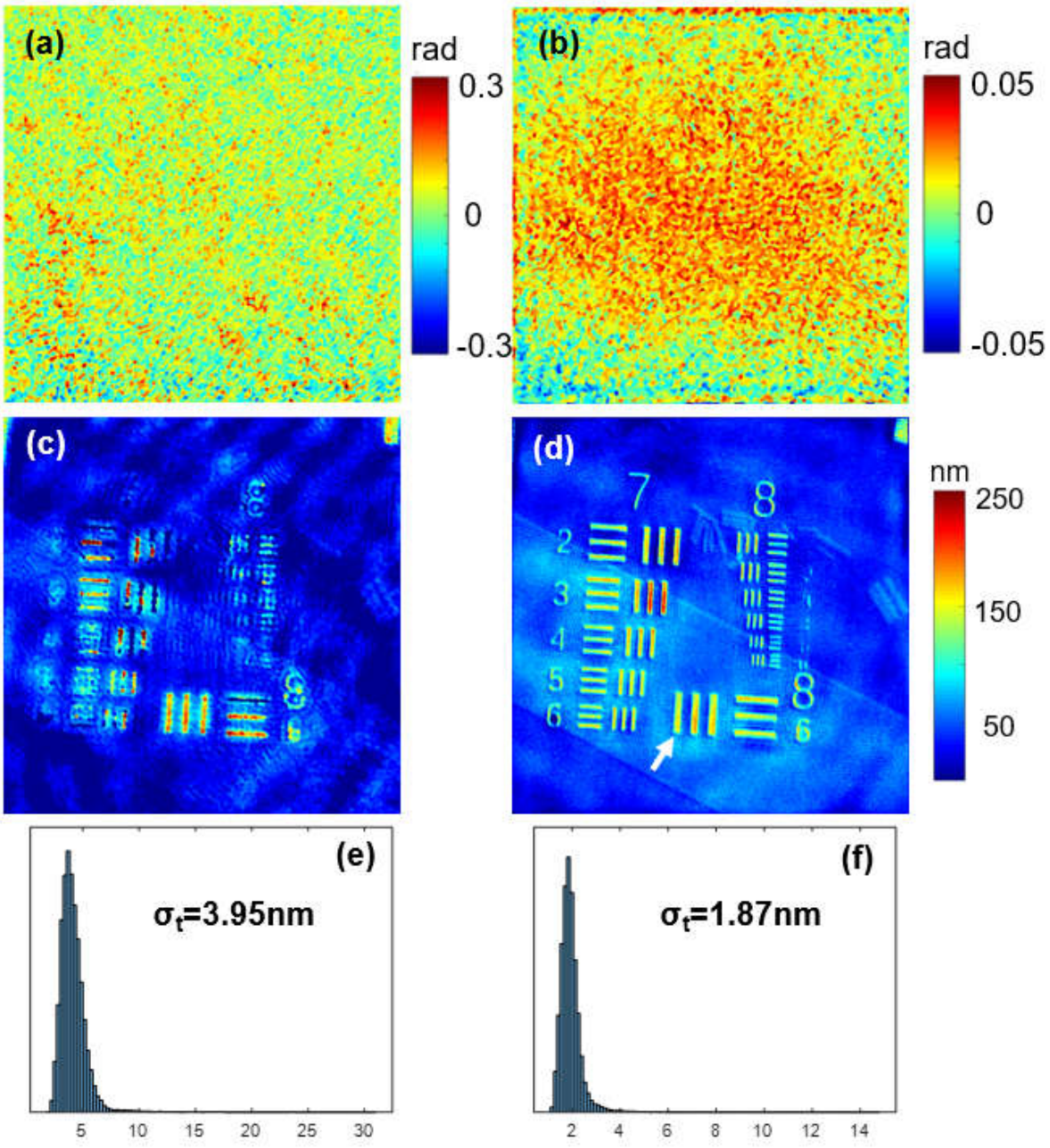

Figure S2. Speckle noise reduction quantification. Phase map of background and subwavelength structure reconstructed (a-c) under normal illumination and (b-d) after synthetic aperture reconstruction. Temporal noise in background (e) under normal illumination and (f) after synthetic aperture reconstruction. After the synthetic aperture reconstruction, the standard deviation of the phase map has reduced from 0.66 rad to 0.1 rad and median of the temporal

noise has reduced from 3.95 nm to 1.87 nm. We attribute this phase noise reduction to the phase mismatch correction and the incoherent addition in the aperture synthesis process. As our physical model precisely models the image formation process, the slowly fluctuating signals, originating from out-of-focal plane regions in the optical path, are eliminated and averaged out.

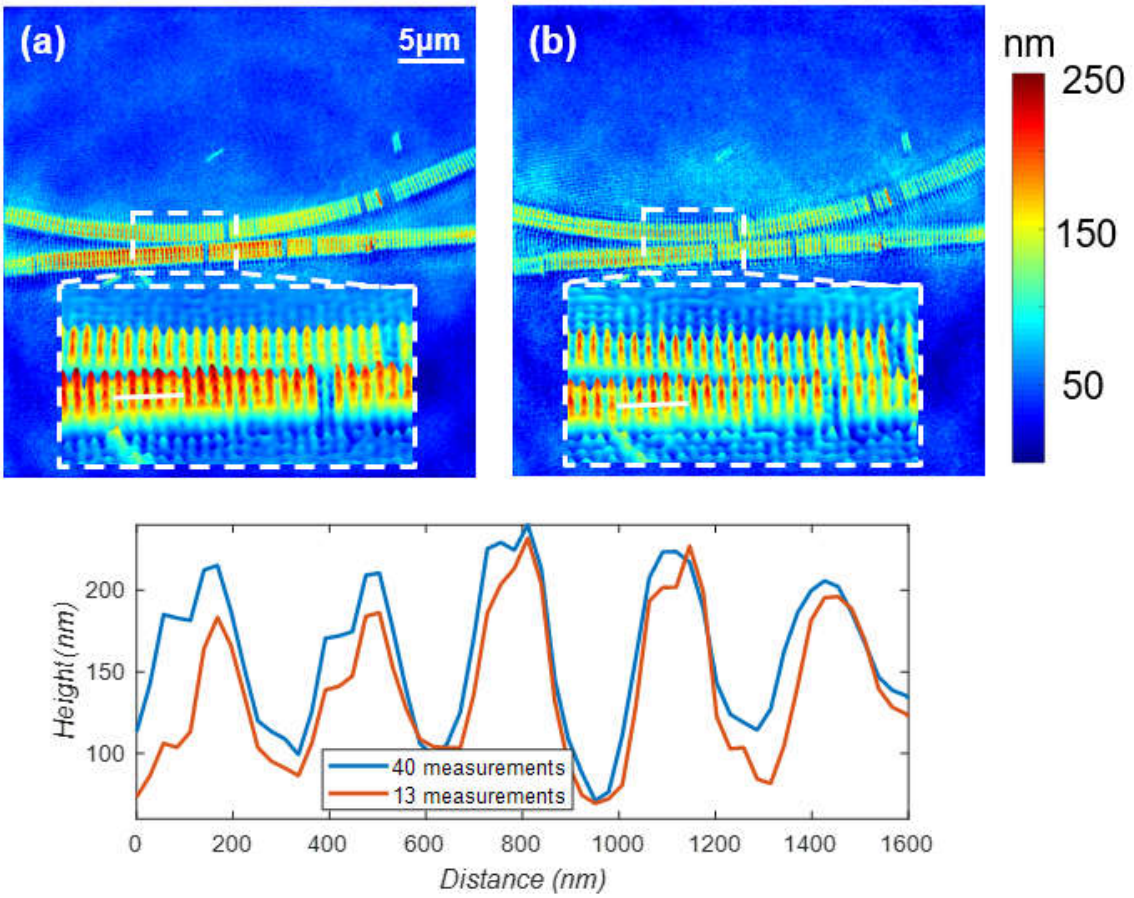

Figure S3. Reconstruction with less scanning angles. Reconstructed height profile using (a) 40 scanning angles and (b) 13 scanning angles; (c) Line profiles along the white line in (a) and (b). An increase in the background noise is observed in (b), but from the retrieved height profile we can still discern the features without losing many details. This comparison shows it is possible to reduce the number of scanning angles by more than 3x, depending on the imaging application requirements.

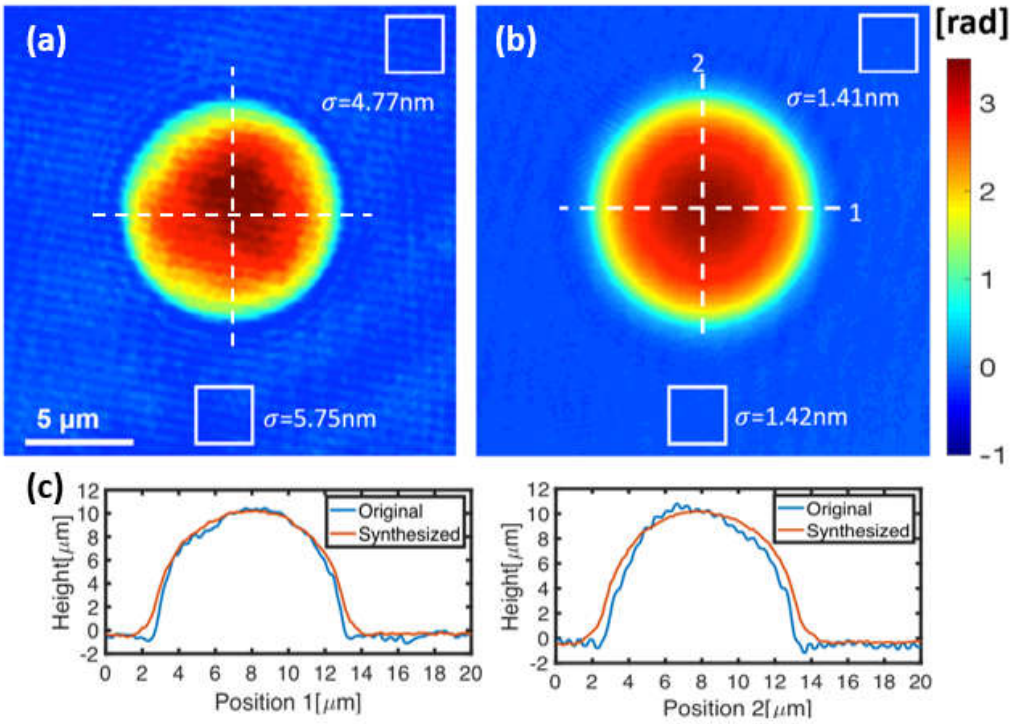

Figure S4. Experimental results on the validation of phase reconstruction accuracy in HISTR-SAPM. (a) The phase map of a 10 μm diameter bead under normal illumination. (b) The phase map reconstructed with HISTR-SAPM for the bead in (a). (c) The height profiles of the bead along line 1 and line 2 obtained from the phase map in (a) and (b). The height values in both cases match well with the theoretical value, while the height profiles after aperture synthesis are smoother and more symmetric due to the reduction of the laser speckle. There is also a reduction in the background noise level in the areas indicated by white boxes.